

Universal Spreading of Conditional Mutual Information in Noisy Random Circuits

Su-un Lee,^{1,*} Changhun Oh,^{1,2} Yat Wong,¹ Senrui Chen,¹ and Liang Jiang^{1,†}

¹*Pritzker School of Molecular Engineering, The University of Chicago, Chicago, IL 60637, USA*

²*Department of Physics, Korea Advanced Institute of Science and Technology, Daejeon 34141, Republic of Korea*
(Dated: May 3, 2024)

We study the evolution of conditional mutual information (CMI) in generic open quantum systems, focusing on one-dimensional random circuits with interspersed local noise. Unlike in noiseless circuits, where CMI spreads linearly while being bounded by the lightcone, we find that noisy random circuits with an error rate p exhibit superlinear propagation of CMI, which diverges far beyond the lightcone at a critical circuit depth $t_c \propto p^{-1}$. We demonstrate that the underlying mechanism for such rapid spreading is the combined effect of local noise and a scrambling unitary, which selectively removes short-range correlations while preserving long-range correlations. To analytically capture the dynamics of CMI in noisy random circuits, we introduce a coarse-graining method, and we validate our theoretical results through numerical simulations. Furthermore, we identify a universal scaling law governing the spreading of CMI.

Introduction.—Understanding information spreading in non-equilibrium quantum systems is central to studying chaotic quantum systems, as well as essential for realizing quantum technologies. For these theoretical and practical purposes, random quantum circuits have served as a fruitful model to study the generic properties of quantum systems. The irreversible growth and spread of entanglement in random quantum circuits have elucidated the mechanisms underpinning quantum thermalization and chaos [1–4], provided useful models for black holes [5–7], and showcased their utility in efficient quantum error-correcting codes [8–10]. However, incorporating noise is essential to enhance the physical relevance and applicability to near-term quantum devices. Thus, random quantum circuits interspersed with decoherence channels have been introduced to describe generic open quantum systems [11–14].

Among various measures characterizing information dynamics, conditional dependence holds fundamental and practical significance in quantum information and many-body physics. It is intimately connected with the classical description of quantum states [15–18], efficient quantum algorithms for state preparations [19, 20], topological orders [21–24], and the information-theoretic measure of mixed-state quantum entanglement [25–27].

Given a state ρ , the direct correlation between the subsystems A and C is quantified by mutual information,

$$I(A : C) = S(A) + S(C) - S(AC), \quad (1)$$

where $S(X) = -\text{Tr}(\rho_X \log_2 \rho_X)$ is the von Neumann entropy of the reduced density matrix ρ_X of the subsystem X . Meanwhile, the dependence of A and C , conditioned on another subsystem B , is captured by conditional mutual information (CMI),

$$I(A : C|B) = S(AB) + S(BC) - S(B) - S(ABC). \quad (2)$$

CMI is associated with approximate recoverability [28, 29], thereby serving as a measure of conditional depen-

dence. The structures of CMI in the states in thermal equilibrium or topologically ordered states have been studied extensively [20, 30, 31]. However, its behavior in dynamical systems remains less understood.

In this Letter, we study the dynamics of CMI in generic open quantum systems. Specifically, we consider quantum circuits that start with a product state and are subjected to random local gates, possibly with noise. We establish that in noiseless circuits, CMI spreads linearly constrained by the lightcone. Introducing noise, however, leads to the rapid spreading of CMI beyond the lightcone. We demonstrate the underlying mechanism for such rapid spreading by showing that the local noise combined with a scrambling unitary selectively removes the short-range correlation while preserving the long-range correlation.

Equipped with the understanding of the non-local spreading of CMI, we study one-dimensional random circuits with interspersed local noise controlled by the error rate p . We introduce *coarse-grained random circuit*, a new theoretical model that admits theoretical and numerical analysis. This model reveals that the higher the error rate within the circuit, the more rapid the spreading of CMI is. Remarkably, the spreading diverges at a critical timestep $t_c \propto p^{-1}$, leading to the entire system becoming conditionally dependent. Furthermore, we analytically identify and numerically validate a universal scaling law governing the spreading of CMI.

Bound of lightcone in noiseless circuits.—We first show that when a quantum circuit is noiseless, the spreading of CMI is bounded by the lightcone. Consider a one-dimensional quantum circuit of N qubits that begins with a product state $\rho^{\text{init}} = \bigotimes_{i=1}^N \rho_i$. We choose two subsets of qubits A and C , and denote B to be $\{1, 2, \dots, N\} \setminus (A \cup C)$ as depicted in Fig. 1(a). We say A and C are lightcone-separated if $\mathcal{L}(A) \cap \mathcal{L}(C) = \emptyset$, where $\mathcal{L}(X)$ is the backward lightcone of X .

Given the output state ρ , suppose A and C are lightcone-separated. We undo the gates outside of $\mathcal{L}(A) \cup \mathcal{L}(C)$ by applying the inverses of those gates suc-

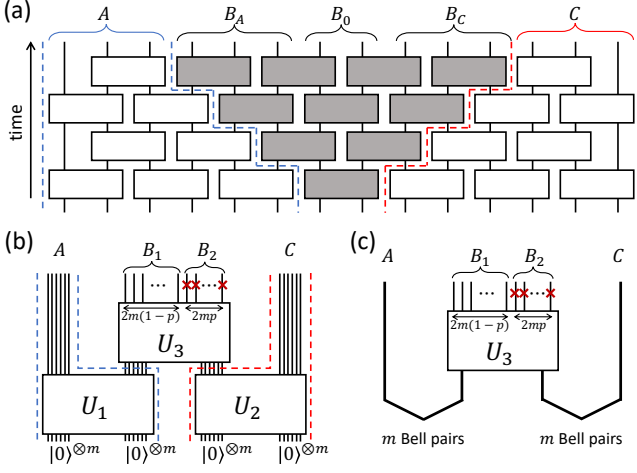


FIG. 1. (a) 1D noiseless quantum circuit. $\mathcal{L}(A)$ and $\mathcal{L}(C)$ are denoted by the regions enclosed by blue and red dashed lines, respectively. The gates outside of $\mathcal{L}(A) \cup \mathcal{L}(B)$ are colored grey. (b) Quantum circuit with noise. After two layers of random Clifford gates, a fraction of p of the qubits in B are completely depolarized. (c) Due to the gates U_1 and U_2 in (b), A and C effectively share m Bell pairs with B , respectively.

cessively. Since those are unitary gates applied only on B , they do not change $I(A : C|B)$. Then, the resultant state σ after undoing those gates takes the form of $\sigma = \sigma_{AB_A} \otimes \sigma_{B_0} \otimes \sigma_{CB_C}$, where B_A (or B_C) denotes the set of qubits that are in the support of $\mathcal{L}(A)$ (or $\mathcal{L}(C)$), and $B_0 = B \setminus (B_A \cup B_C)$. This results in $I(A : C|B) = 0$ from the definition of CMI. Therefore, the spreading of CMI is bounded by the lightcone in noiseless circuits.

Selective removal of correlation.—Contrarily, noisy circuits can spread CMI into lightcone-separated regions. Here, we show that this rapid spreading stems from the fact that local noises, along with the scrambling unitary, selectively destroy the short-range correlation while preserving the long-range correlation. To understand this, we consider a quantum circuit of four blocks consisting of $m \gg 1$ qubits, as depicted in Fig. 1(b). We denote the first and last blocks by A and C , respectively, and the two blocks in the middle by B . Starting from the product state $|0\rangle^{\otimes 4m}$, the two halves of the system undergo random Clifford gates U_1 and U_2 , respectively. Then, we apply another random Clifford gate U_3 on B . Finally, we completely depolarize a fraction of p of the qubits in B :

$$\rho_{ABC} \mapsto \text{Tr}_{B_2} \rho_{ABC} \otimes \frac{\mathbb{1}_{B_2}}{d_{B_2}}, \quad (3)$$

where B_2 represents the depolarized qubits, and $B_1 = B \setminus B_2$. Here, d_{B_2} is the Hilbert space dimension of B_2 . Note that A and C are lightcone-separated.

A key observation is that depolarizing B_2 only removes the short-range correlation $I(A : B)$ but not the long-range correlation $I(A : BC)$, as long as $p < 1/2$. Initially, random Clifford gates U_1 and U_2 almost max-

imally entangle the first and last two blocks because of the large dimensionality [32, 33]. This effectively forms m Bell pairs shared by A and B , and another m Bell pairs shared by B and C [Fig. 1(c)]. Therefore, noting that each Bell pair counts two in mutual information, $I(A : B) = I(B : C) = 2m$ and $I(A : BC) = I(AB : C) = 2m$ before we depolarize B_2 .

Then, given $p < 1/2$, the complete depolarization of B_2 preceded by U_3 decreases $I(A : B)$ by $4mp$. To see this, note that before the depolarization, U_3 nearly maximally entangle AB_1 with B_2C [32, 33], resulting in $S(AB_1) = 2mp + m$. Meanwhile, $S(A) = m$ and $S(B_1) = 2m(1 - p)$ as both A and B_1 are maximally entangled with the other subsystems. These leads to $I(A : B_1) = 2m(1 - 2p)$, and thus,

$$I(A : B) = 2m(1 - 2p) \quad (4)$$

after we depolarize B_2 .

Contrarily, depolarizing B_2 does not decrease $I(A : BC)$. Before we depolarize B_2 , the decoupling inequality [5, 32, 34, 35] states that due to the scrambling unitary U_3 , A and B_2 are almost decoupled when $p < 1/2$:

$$\mathbb{E}_{U_3} \left[\left\| \rho_{AB_2}(U_3) - \rho_A \otimes \frac{\mathbb{1}_{B_2}}{d_{B_2}} \right\|_1 \right] \leq 2^{-m(1-2p)}, \quad (5)$$

where $\rho_{AB_2}(U_3)$ is the reduced density matrix of AB_2 after applying U_3 . Here, $\|\cdot\|_1$ denotes the trace norm, and \mathbb{E}_{U_3} represents averaging over random Clifford gates on B . The decoupling of A and B_2 ensures the recovery of the m Bell pairs with A from B_1C with probability $1 - \mathcal{O}(2^{-m(1-2p)})$ [36, 37]. Therefore, any operation on B_2 does not decrease $I(A : BC)$ in large m limit. As a result,

$$I(A : BC) = 2m, \quad (6)$$

after we depolarize B_2 .

Eqs. (4) and (6) confirm that the loss of B_2 preceded by U_3 selectively destroys $I(A : B)$ while preserving $I(A : BC)$. Importantly, by the chain rule $I(A : C|B) = I(A : BC) - I(A : B)$, CMI is the discrepancy between the short-range and long-range correlations, resulting in $I(A : C|B) = 4mp$. Consequently, the lightcone-separated regions A and C share a non-zero CMI after the depolarization. See Ref. [38] for an alternative derivation based on the stabilizer formalism.

Coarse-grained random circuit.—With the understanding of the non-local spreading of CMI, we study the dynamics of CMI in noisy random circuits. Inspired by Ref. [39], we introduce the coarse-grained random circuit, a new model of noisy random circuits [Fig. 2(a)]. This circuit comprises a one-dimensional array of $N \gg 1$ blocks, each containing m qubits. Therefore, the coarse-graining factor m determines the local dimensionality. Starting

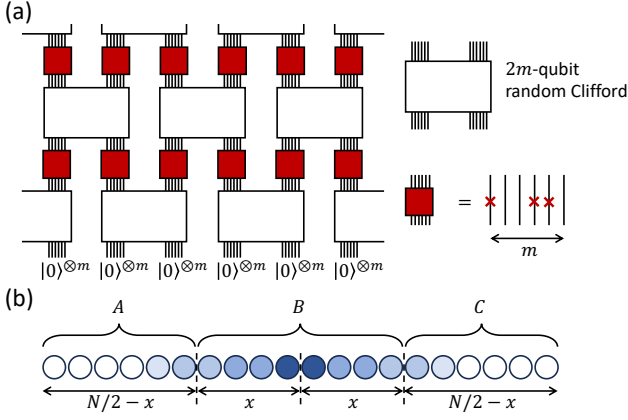


FIG. 2. (a) Coarse-grained random circuit. Beginning with a product state, we alternately apply random Clifford gates to the neighboring blocks, followed by heralded depolarizing channels. (b) At each timestep, the system is divided into A , B , and C to calculate $I^{\text{norm}}(A : C|B)$.

with a product state $|0\rangle^{\otimes mN}$, we alternately apply $2m$ -qubit random Clifford gates on the even and odd pairs of the adjacent blocks. After each layer of unitary gates, we apply *heralded depolarizing channel* on each qubit with an error rate p . A heralded depolarizing channel acting on qubit i with an error rate p is defined by completely depolarizing qubit i with probability p :

$$\rho \mapsto \begin{cases} \text{Tr}_i \rho \otimes \mathbb{1}_i/2 & \text{with Prob. of } p, \\ \rho & \text{with Prob. of } 1 - p, \end{cases} \quad (7)$$

which is a simplified version of the depolarizing channel—this noise model is identical to the depolarizing channel, except the spacetime location of depolarization is determined for each circuit realization [38]. Every timestep, we calculate the normalized CMI $I^{\text{norm}}(A : C|B) = I(A : C|B)/m$, averaged over circuit realizations. Here A is the first $N/2 - x$ blocks, B is the $2x$ blocks in the middle, and C is the last $N/2 - x$ blocks [Fig. 2(b)]

The choice of unitary gates and noise channel is due to their classical simulability and analytical convenience, as Clifford gates and complete depolarization are efficiently described in the stabilizer formalism [40, 41]. Importantly, since the Clifford group forms a unitary 3-design [42, 43], the averaged quantities are expected to be similar to those from the Haar random circuit or generic chaotic models [3, 4]. Moreover, despite the simplification, the heralded depolarizing channel showcases qualitative similarity to the depolarizing channel when combined with random gates [11, 12].

Since the qubits are kept depolarized, the system's entropy increases until the state becomes maximally mixed. Roughly, each qubit is scrambled with $\sim m/p$ qubits before being depolarized. Thus, given a sufficiently small error rate, each qubit becomes maximally entangled with

others before its depolarization. This results in two depolarized qubits for each depolarization event [44]. Therefore, at timestep t , $m(1 - 2pt)$ qubits remain undepolarized in each block, and the system becomes almost maximally mixed at the critical timestep $t_c = 1/2p$.

Fig. 3(a) presents the evolution of $I^{\text{norm}}(A : C|B)$ for finite m (numerical) and $m \rightarrow \infty$ (analytical) with various error rates. In noiseless circuits, $I(A : C|B) = 0$ for $x > t$, since A and C are lightcone-separated. We observe that the spreading of $I(A : C|B)$ becomes faster as we increase the coarse-graining factor m . This is because there are non-negligible portions of Clifford gates that do not maximally entangle the two blocks when m is small, and that portion shrinks as m grows [32, 33].

Contrarily, introducing noise results in $I(A : C|B)$ attaining non-zero values in regions well beyond the lightcone, attributed to the selective removal of short-range correlations. This phenomenon can be analytically captured in the limit $m \rightarrow \infty$ [38]. As seen in Eq. (6), depolarization channels cannot decrease the long-range correlation $I(A : BC)$ as long as less than half of the qubits are depolarized. Meanwhile, at every two timesteps, a $2m$ -qubit random Clifford gate is applied between A and B , thereby increasing $I(A : BC)$. Since the random Clifford gate maximally generates entanglement in the large m limit and that there are $2m(1 - 2pt)$ non-depolarized qubits on its support, $I(A : BC)$ increases by $4m(1 - 2pt)$ at every two timesteps. Therefore, by integrating this increment,

$$I(A : BC) = 2mt(1 - pt), \quad (8)$$

for $t < t_c$. In contrast, using a similar method for deriving Eq. (4), we show in Ref. [38] that the short-range correlation $I(A : B)$ is upper bounded by $2m(1 - 2pt)x$, resulting in

$$I(A : B) = \min\{2m(1 - 2pt)x, I(A : BC)\}. \quad (9)$$

Therefore, by the chain rule,

$$I^{\text{norm}}(A : C|B) = \max\{2t(1 - pt) - 2(1 - 2pt)x, 0\}, \quad (10)$$

given $t < t_c$. Note that $I(A : C|B) = 0$ when $t > t_c$ as the system becomes maximally mixed.

As we increase the separation x , $I^{\text{norm}}(A : C|B)$ decays until it becomes zero. We define $x_{\text{dec}}(t)$ as the separation x at which $I(A : C|B)$ begins to be zero for $t < t_c$, indicating the spreading front of CMI. Then, Eq. (10) demonstrates that

$$x_{\text{dec}}(t) = \frac{t(1 - pt)}{1 - 2pt}. \quad (11)$$

One can see that the spreading becomes more rapid as we increase the error rate p . Notably, the spreading front $x_{\text{dec}}(t)$ diverges as $t \rightarrow t_c$. Therefore, a non-negligible amount of conditional dependence spreads out to the

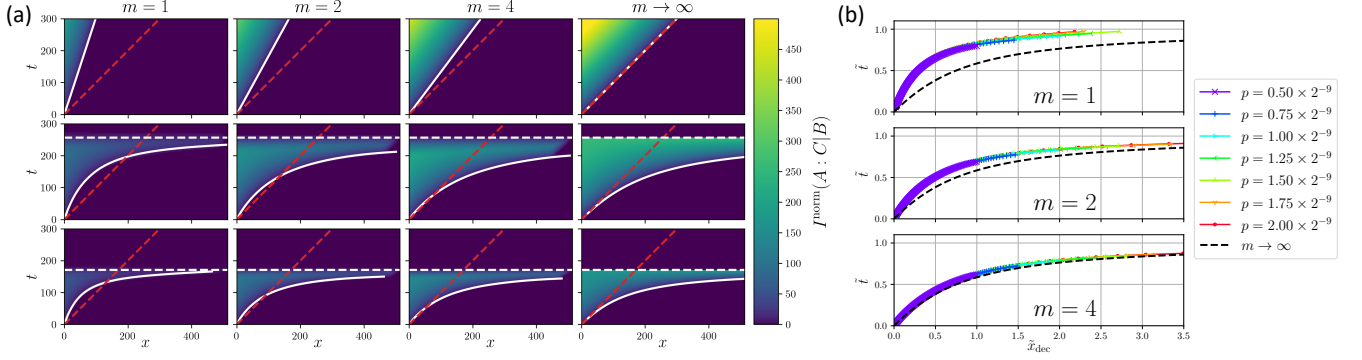


FIG. 3. (a) Evolution of $I^{\text{norm}}(A:C|B)$ with various circuit depths t and separation lengths x . The first three columns present the numerical results for the finite coarse-graining factors m , whereas the last column shows the analytical result from Eq. (10). The first row is the result of noiseless circuits ($p = 0$), with subsequent rows for $p = 1.0 \times 10^{-9}$ and $p = 1.5 \times 10^{-9}$, respectively. Red dashed lines mark the limit set by lightcone ($x = t$). For noisy cases ($p > 0$), t_c is marked by white dashed lines. White solid lines represent $x_{\text{dec}}(t)$. (b) $\tilde{x}_{\text{dec}}(\tilde{t})$ with various error rates p and coarse-graining factors m . The theoretical result for $m \rightarrow \infty$ is depicted as black dashed lines. The numerical results in (a) and (b) are based on averages from 1000 circuit realizations with $N = 2^{10}$.

entire system right before the state becomes maximally mixed.

Our derivations of the rapid spreading and critical behavior of CMI are based on the limit of $m \rightarrow \infty$, where the long-range correlation is perfectly protected from the local noise while the short-range correlation keeps decreasing. However, we emphasize that this selective removal of short-range correlation also emerges in the cases of finite m as long as the error rate is sufficiently low. As seen in Fig. 3(a), those features of rapid spreading and divergence at t_c are observed in the numerical results of the finite m .

Universal scaling law.—Remarkably, the dynamics of CMI exhibit a universal scaling law. Specifically, we consider the following rescaling:

$$\tilde{t} = 2pt, \quad (12)$$

$$\tilde{x} = 2px, \quad (13)$$

$$\tilde{I}^{\text{norm}}(A:C|B) = pI^{\text{norm}}(A:C|B). \quad (14)$$

This rescaling makes Eqs. (10) and (11) error-rate-independent, demonstrating the universal scaling law:

$$\tilde{I}^{\text{norm}}(A:C|B) = \max\{0, \tilde{t}(1 - \tilde{t}/2) - (1 - \tilde{t})\tilde{x}\}, \quad (15)$$

$$\tilde{x}_{\text{dec}}(\tilde{t}) = \frac{\tilde{t}(1 - \tilde{t}/2)}{1 - \tilde{t}}, \quad (16)$$

for $\tilde{t} < 1$, where $\tilde{x}_{\text{dec}}(\tilde{t}) = 2px_{\text{dec}}(\tilde{t}/2p)$. Fig. 3(b) presents rescaled spreading fronts $\tilde{x}_{\text{dec}}(\tilde{t})$ from the numerical results of finite m along with the analytical result of $m \rightarrow \infty$ in Eq. (16). For a fixed coarse-graining factor m , the spreading fronts across varying error rates collapse into a single curve, affirming the applicability of the universal scaling law even for the circuit with finite m . As we increase m , the collapsed curve $\tilde{x}_{\text{dec}}(\tilde{t})$ approaches the analytical result.

Note that slight deviations exist in the rescaled spreading fronts $\tilde{x}_{\text{dec}}(\tilde{t})$ for large p values when $m = 1$. In the circuits with finite m , local noise still selectively removes short-range correlations $I(A:B)$. However, it can reduce $I(A:BC)$ for a small amount since the correlation is scrambled into a finite number of qubits. This introduces higher-order effects of p on $I(A:BC)$, leading to small deviations in $\tilde{x}_{\text{dec}}(\tilde{t})$. Fig. 3(b) shows that such higher-order effects are suppressed as we decrease the p or increase m .

Discussion.—Rapid spreading of CMI shows that causally separated regions become conditionally dependent. However, it is important to remark that although the non-trivial correlation extends far beyond the lightcone, our findings do not conflict with the Lieb-Robinson bound or the principles of causality [45–47], as local observers in A and C cannot detect $I(A:C|B)$.

Meanwhile, the divergence of $x_{\text{dec}}(t)$ as $t \rightarrow t_c$ indicates that CMI spreads into the entire system. We emphasize that this pervasive conditional dependence implies that the multipartite quantum correlation extends throughout the entire system. Specifically, at the critical timestep, we show in Ref. [38] that no matter how largely separated A and C are, measuring B and heralding the measurement outcome to A and C generate Bell pairs shared by A and C . Here, CMI acts as an upper bound of the number of generatable Bell pairs.

This result bears similarities to entanglement swapping [48], as it also generates entanglement between two distant regions through measurement and heralding the outcome. However, a fundamental difference exists. In the entanglement-swapping protocol, two separate Bell pairs between A , B , and B , C are prepared, and the measurement on B generates entanglement between A and C . In our case, however, we have inseparable mul-

tipartite correlations among A , B , and C , and the measurement on B reduces them into entanglement between A and C [38].

Finally, we remark that prior studies have shown that there exist constant depth circuits acting on a product state that generate CMI between arbitrarily large distant regions [24, 49–51]. Our findings further extend this understanding by demonstrating that the formation of long-distance conditional dependence also emerges within noisy random circuits without designing a sophisticated circuit to achieve it.

Note added.—Upon completion of our study, we became aware of related independent work [52], which we believe complements our findings.

We acknowledge support from the ARO(W911NF-23-1-0077), ARO MURI (W911NF-21-1-0325), AFOSR MURI (FA9550-19-1-0399, FA9550-21-1-0209, FA9550-23-1-0338), DARPA (HR0011-24-9-0359, HR0011-24-9-0361), NSF (OMA-1936118, ERC-1941583, OMA-2137642, OSI-2326767, CCF-2312755), NTT Research, Packard Foundation (2020-71479), and the Marshall and Arlene Bennett Family Research Program. This material is based upon work supported by the U.S. Department of Energy, Office of Science, National Quantum Information Science Research Centers. S.L. is partially supported by Kwanjeong Educational Foundation. The authors are also grateful for the support of the University of Chicago’s Research Computing Center for assistance with the numerical experiments carried out in this work.

* suun@uchicago.edu

† liang.jiang@uchicago.edu

- [1] J. M. Deutsch, Phys. Rev. A **43**, 2046 (1991).
- [2] M. Srednicki, Phys. Rev. E **50**, 888 (1994).
- [3] A. Nahum, J. Ruhman, S. Vijay, and J. Haah, Phys. Rev. X **7**, 031016 (2017).
- [4] A. Nahum, S. Vijay, and J. Haah, Phys. Rev. X **8**, 021014 (2018).
- [5] P. Hayden and J. Preskill, J. High Energy Phys. **2007**, 120 (2007).
- [6] Y. Sekino and L. Susskind, J. High Energy Phys. **2008**, 065 (2008).
- [7] P. Hosur, X.-L. Qi, D. A. Roberts, and B. Yoshida, J. High Energy Phys. **2016**, 4 (2016).
- [8] W. Brown and O. Fawzi, in *2013 IEEE International Symposium on Information Theory* (2013) pp. 346–350.
- [9] W. Brown and O. Fawzi, Commun. Math. Phys. **340**, 867 (2015).
- [10] M. J. Gullans, S. Krastanov, D. A. Huse, L. Jiang, and S. T. Flammia, Phys. Rev. X **11**, 031066 (2021).
- [11] K. Noh, L. Jiang, and B. Fefferman, Quantum **4**, 318 (2020).
- [12] Z. Li, S. Sang, and T. H. Hsieh, Phys. Rev. B **107**, 014307 (2023).
- [13] Y.-L. Zhang, Y. Huang, and X. Chen, Phys. Rev. B **99**, 014303 (2019).
- [14] T. Schuster and N. Y. Yao, Phys. Rev. Lett. **131**, 160402 (2023).
- [15] A. Molnar, N. Schuch, F. Verstraete, and J. I. Cirac, Phys. Rev. B **91**, 045138 (2015).
- [16] M. B. Hastings, Phys. Rev. B **76**, 201102 (2007).
- [17] M. S. Leifer and D. Poulin, Annals of Physics **323**, 1899 (2008).
- [18] D. Poulin and M. B. Hastings, Phys. Rev. Lett. **106**, 080403 (2011).
- [19] F. G. S. L. Brandão and M. J. Kastoryano, Commun. Math. Phys. **365**, 1 (2019).
- [20] K. Kato and F. G. S. L. Brandão, Commun. Math. Phys. **370**, 117 (2019).
- [21] A. Kitaev and J. Preskill, Phys. Rev. Lett. **96**, 110404 (2006).
- [22] M. Levin and X.-G. Wen, Phys. Rev. Lett. **96**, 110405 (2006).
- [23] I. H. Kim, *Conditional independence in quantum many-body systems*, Ph.D. thesis, California Institute of Technology (2013).
- [24] I. H. Kim, M. Levin, T.-C. Lin, D. Ranard, and B. Shi, Phys. Rev. Lett. **131**, 166601 (2023).
- [25] M. Christandl and A. Winter, Journal of Mathematical Physics **45**, 829 (2004).
- [26] F. G. S. L. Brandão, M. Christandl, and J. Yard, Commun. Math. Phys. **306**, 805 (2011).
- [27] K. P. Seshadreesan and M. M. Wilde, Phys. Rev. A **92**, 042321 (2015).
- [28] O. Fawzi and R. Renner, Commun. Math. Phys. **340**, 575 (2015).
- [29] D. Petz, Rev. Math. Phys. **15**, 79 (2003).
- [30] T. Kuwahara, K. Kato, and F. G. Brandão, Phys. Rev. Lett. **124**, 220601 (2020).
- [31] A. W. Harrow, S. Mehraban, and M. Soleimanifar, in *Proceedings of the 52nd Annual ACM SIGACT Symposium on Theory of Computing*, STOC 2020 (Association for Computing Machinery, New York, NY, USA, 2020) pp. 378–386.
- [32] J. Preskill, “Lecture notes for physics 219: Quantum Computation,” (2018).
- [33] H. Apel, T. Kohler, and T. Cubitt, J. High Energy Phys. **2022**, 52 (2022).
- [34] A. Abeyesinghe, I. Devetak, P. Hayden, and A. Winter, Proc. Math. Phys. Eng. Sci. **465**, 2537 (2009).
- [35] P. Hayden, M. Horodecki, A. Winter, and J. Yard, Open Syst. Inf. Dyn. **15**, 7 (2008).
- [36] B. Yoshida and A. Kitaev, “Efficient decoding for the Hayden-Preskill protocol,” (2017), arXiv:1710.03363.
- [37] B. Yoshida, “Recovery algorithms for Clifford Hayden-Preskill problem,” (2022), arXiv:2106.15628.
- [38] See Supplemental Materials for the derivation of the analytical result, detailed numerical results, the protocol to generate Bell pairs between an arbitrary distance at $t \rightarrow t_c$, and further discussion on the heralded depolarizing channel, which includes Refs. [53–56].
- [39] S. Choi, Y. Bao, X.-L. Qi, and E. Altman, Phys. Rev. Lett. **125**, 030505 (2020).
- [40] D. Gottesman, “The Heisenberg Representation of Quantum Computers,” (1998), arXiv:quant-ph/9807006.
- [41] S. Aaronson and D. Gottesman, Phys. Rev. A **70**, 052328 (2004).
- [42] Z. Webb, Quantum Info. Comput. **16**, 1379 (2016).
- [43] H. Zhu, Phys. Rev. A **96**, 062336 (2017).

- [44] If we depolarize one of the qubits of a Bell pair $\frac{1}{\sqrt{2}}(|00\rangle + |11\rangle)$, both qubits are depolarized.
- [45] E. H. Lieb and D. W. Robinson, Commun.Math. Phys. **28**, 251 (1972).
- [46] S. Bravyi, M. B. Hastings, and F. Verstraete, Phys. Rev. Lett. **97**, 050401 (2006).
- [47] C.-F. A. Chen, A. Lucas, and C. Yin, Rep. Prog. Phys. **86**, 116001 (2023).
- [48] C. H. Bennett, G. Brassard, C. Crépeau, R. Jozsa, A. Peres, and W. K. Wootters, Phys. Rev. Lett. **70**, 1895 (1993).
- [49] L. Zou and J. Haah, Phys. Rev. B **94**, 075151 (2016).
- [50] D. J. Williamson, A. Dua, and M. Cheng, Phys. Rev. Lett. **122**, 140506 (2019).
- [51] K. Kato and F. G. S. L. Brandão, Phys. Rev. Research **2**, 032005 (2020).
- [52] Y. Zhang and S. Gopalakrishnan, “Nonlocal growth of quantum conditional mutual information under decoherence,” (2024), arXiv:2402.03439.
- [53] K. M. R. Audenaert and M. B. Plenio, New J. Phys. **7**, 170 (2005).
- [54] Y. Li, X. Chen, and M. P. A. Fisher, Phys. Rev. B **100**, 134306 (2019).
- [55] S. Sang, Z. Li, T. H. Hsieh, and B. Yoshida, PRX Quantum **4**, 040332 (2023).
- [56] T. M. Cover and J. A. Thomas, *Elements of information theory*, 2nd ed. (Wiley-Interscience, Hoboken, N.J, 2006).

Supplemental Material for “Universal Spreading of Conditional Mutual Information in Noisy Random Circuits”

Su-un Lee,¹ Changhun Oh,^{1,2} Yat Wong,¹ Senrui Chen,¹ and Liang Jiang¹

¹*Pritzker School of Molecular Engineering, The University of Chicago, Chicago, IL 60637, USA*

²*Department of Physics, Korea Advanced Institute of Science and Technology, Daejeon 34141, Republic of Korea*

(Dated: May 3, 2024)

CONTENTS

| | |
|--|----|
| I. Preliminaries | 1 |
| A. Stabilizer formalism | 1 |
| B. Clipped gauge | 2 |
| II. Derivation of the analytical result | 3 |
| A. Random stabilizer state and maximal scrambling ansatz | 3 |
| B. Four-block example | 4 |
| C. Coarse-grained circuit | 6 |
| III. Detailed numerical results | 8 |
| IV. Generating entanglement between a large distance | 10 |
| V. Further discussion on the heralded depolarizing channel | 12 |
| References | 13 |

I. PRELIMINARIES

A. Stabilizer formalism

Stabilizer formalism provides a compact and efficient way to represent a wide class of quantum states and their dynamics, utilizing a stabilizer group [1, 2]. A stabilizer group \mathcal{S} is an Abelian subgroup of the Pauli group \mathcal{P}_N of N qubits with the constraint of $-I \notin \mathcal{S}$. Let $G = \{g_1, g_2, \dots, g_K\}$ be a generating set of the stabilizer group \mathcal{S} , i.e., $\mathcal{S} = \langle g_1, g_2, \dots, g_K \rangle$, where K is the number of the generators. A stabilizer state ρ corresponding to \mathcal{S} is a uniform mixture over the vector space spanned by 2^{N-K} simultaneous eigenstates of \mathcal{S} . The state ρ is explicitly written as

$$\rho = \frac{1}{2^N} \sum_{g \in \mathcal{S}} g = \frac{1}{2^{N-K}} \prod_{k=1}^K \frac{\mathbb{1} + g_k}{2}. \quad (\text{S1})$$

Therefore, we can efficiently express the dynamics of the state ρ only by keeping track of the generating set G . Since ρ is a uniform mixture over 2^{N-K} orthonormal states, the von Neumann entropy $S_\rho = -\text{Tr}(\rho \log_2 \rho)$ is $N - K$. Note that ρ is a pure state when $K = N$ and a maximally mixed state when $K = 0$.

For notational convenience, we introduce a *stabilizer tableau* to represent G , which is a matrix of K rows and N columns. The k -th row is assigned to the generator $g_k \in G$, and in that row, the element at i -th column is the Pauli operator applied by g_k to the i -th qubit. To have a complete description of G , an additional array of K entities is needed to store the overall phases of each generator. However, we disregard these phases as they are irrelevant to the amount of correlation in the state. Additionally, for a stabilizer group \mathcal{S} , note that the corresponding stabilizer tableau is not unique, introducing a gauge degree of freedom. One such example is row permutation; the stabilizer tableau still represents the same generating set G after the rows are permuted. Another degree of freedom is row multiplication, where multiplying one row by another alters the generating set, but the resultant generating set still generates the same stabilizer group \mathcal{S} .

When a Clifford gate U is applied to the state ρ , we simply update each row from g_k to Ug_kU^\dagger , since $G' = \{Ug_1U^\dagger, Ug_2U^\dagger, \dots, Ug_KU^\dagger\}$ represents the resultant state $U\rho U^\dagger$. Another useful operation is complete depolarization. Complete depolarization of the qubit i maps the state ρ into $\text{Tr}_i \rho \otimes \mathbb{1}_i/2$, where $\mathbb{1}_i$ is the identity operator acting on the qubit i . To apply complete depolarization to the qubit i for a given stabilizer tableau, there are three cases to consider:

Case 1. Every element of the i -th column is $\mathbb{1}$. In this case, the complete depolarization does not change the stabilizer tableau.

Case 2. If there is only one type of nontrivial Pauli operator on the i -th column, suppose k -th row contains this nontrivial Pauli operator at the i -th column. Then, perform row reduction by multiplying other rows with the k -th row, ensuring every row except for the k -th row has $\mathbb{1}$ on the i -th column. Finally, remove the k -th row.

Case 3. If there are more than two kinds of nontrivial Pauli operators on the i -th column, let the k_1 -th and k_2 -th row have different nontrivial Pauli operators at the i -th column. Perform the row reduction by multiplying other rows with the k_1 -th and k_2 -th row, ensuring every row except those two rows has $\mathbb{1}$ on the i -th column. Finally, remove the k_1 -th and k_2 -th rows.

In summary, complete depolarization reduces the number of rows, and the extent of this reduction varies, thereby increasing the entropy. See Ref. [3] for a detailed explanation of complete depolarization in the stabilizer formalism.

The last useful operation introduced here is a measurement with a Pauli observable. Suppose a generating set $G = \{g_1, g_2, \dots, g_K\}$ of a stabilizer group \mathcal{S} that corresponds to a stabilizer state is given. After the measurement with a Pauli observable g , we update G as follows:

Case 1. If $g \in \mathcal{S}$ or $-g \in \mathcal{S}$, then G is unaffected. The measurement outcome is $+1$ when $g \in \mathcal{S}$, and otherwise, the outcome is -1 .

Case 2. If $[g, g_i] = 0$ for all $g_i \in G$ but $g \notin \mathcal{S}$, then the measurement outcome is $+1$ or -1 with equal probability. If the outcome is ± 1 , then we add $\pm g$ in G : $G = \{\pm g, g_1, g_2, \dots, g_K\}$.

Case 3. If g anticommutes with some of the generators in G , then the measurement outcome is $+1$ or -1 with equal probability. Let g_1 be one of such generators. By multiplying the other generators that are anticommuting with g by g_1 , we make g_1 the only generator that anticommutes with g . Then, if the outcome is ± 1 , we replace g_1 in G with $\pm g$: $G = \{\pm g, g_2, \dots, g_K\}$.

Note that for the last two cases, the measurement outcome only determines the overall phase of the generator, which is disregarded in this work.

B. Clipped gauge

As mentioned, two different generating sets can generate the same stabilizer group, and thus, there is a gauge degree of freedom in choosing the corresponding generating set G . The *clipped gauge* is a specific choice of generating set that is useful for analyzing correlations in one-dimensional systems. The clipped gauge is first introduced in Ref. [4], with detailed explanations available in the Appendix of Ref. [5].

Consider an N -qubit system arranged in a one-dimensional array, and suppose a generating set G that corresponds to an $K \times N$ stabilizer tableau is given. For $k = 1, 2, \dots, K$, define the left (or right) endpoint $l(k)$ (or $r(k)$) as the index of the first (or last) column that has a non-trivial element on the k -th row. Additionally, define $\rho_l(i)$ (or $\rho_r(i)$) as the number of rows that have i as their left (or right) endpoint. The choice of the generating set G of the stabilizer group is said to be in the clipped gauge if, for $i = 1, 2, \dots, N$,

- (i) $\rho_l(i) + \rho_r(i) \leq 2$, and
- (ii) if $\rho_l(i) = 2$ or $\rho_r(i) = 2$, then the two rows that have their endpoint at i should have different Pauli operators on the i -th column.

Importantly, it is possible to achieve these two conditions of the clipped gauge for any stabilizer state. The clipping algorithm consists of two parts: First, we make the stabilizer tableau in the row-reduced echelon form (RREF) through Gaussian elimination [3]. Secondly, we transform the tableau into a lower triangular form by performing row-reduction on the right endpoints without affecting the left endpoints. More explicitly, starting from $i = K$ up to $i = 2$, we utilize the i -th row to eliminate the $r(i)$ -th column of j -th rows for $j < i$ [5]. For analytical convenience, we permute

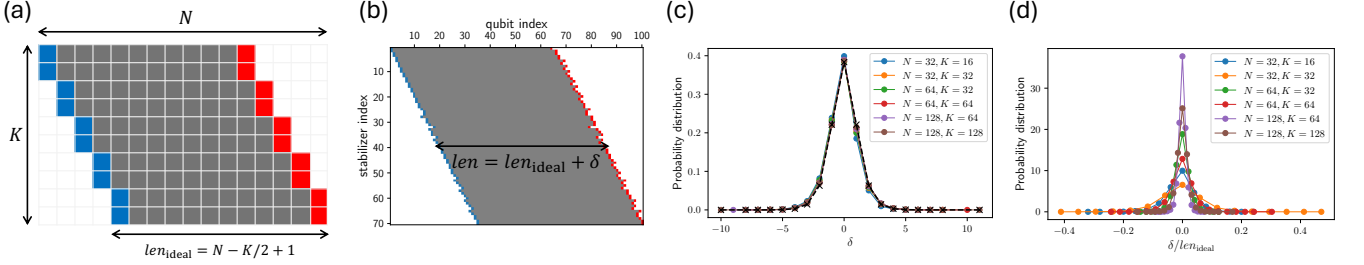


FIG. S1. (a) Stabilizer tableau of the maximal scrambling ansatz. Each row has left and right endpoints marked in blue and red, respectively. The elements between these endpoints are grey, and the elements outside the endpoints are 1 and are colored white. Each row has the length of $len_{ideal} = N - K/2 + 1$. (b) An example of a clipped gauge of a random stabilizer state of $N = 100$ qubits with $K = 70$ stabilizer generators. The length of each row is close to that of maximal scrambling ansatz len_{ideal} with a small fluctuation δ . (c) Distribution of the lengths of stabilizers of random stabilizer states in clipped gauge. The distributions of various values of N and K are presented, and each distribution is averaged over 1000 random stabilizer states. The deviation of the length of the stabilizer generators from that of the maximal scrambling ansatz len_{ideal} is regardless of the values N and K . The black dashed line denotes the fitted line $y = A \text{sech}^2(Bx)$ from the data with $N = 128$ and $K = 128$, indicating that a large deviation is exponentially unlikely. (d) Distribution of δ/len_{ideal} . Since the deviation of the length of the stabilizer generators from len_{ideal} is independent of N and K , it is negligible when compared to the value of len_{ideal} in the large N limit.

the rows so that $l(i) + r(i) \leq l(j) + r(j)$ for $i < j$ so that the mid-point is monotonically increasing with the row index.

The clipped gauge is particularly useful when studying correlations in stabilizer states. Specifically, for two neighboring contiguous regions A and B , with A on the left and B on the right, it is known that [6]

$$I(A : B) = |\{k : l(k) \in A \text{ and } r(k) \in B\}|. \quad (\text{S2})$$

Furthermore, consider two contiguous regions A and C that are separated by another region B . Then, by applying the chain rule of mutual information $I(A : BC) = I(A : B) + I(A : C|B)$, we have

$$I(A : B|C) = |\{k : l(k) \in A \text{ and } r(k) \in C\}|. \quad (\text{S3})$$

Given a stabilizer tableau in the clipped gauge, we define the length of the k -th stabilizer generator as

$$len(k) = r(k) - l(k) + 1. \quad (\text{S4})$$

Then, by Eq. (S3), we see that a non-zero conditional mutual information (CMI) between largely separated regions means the presence of stabilizer generators with a large length in the clipped gauge.

II. DERIVATION OF THE ANALYTICAL RESULT

The analytical results presented in the main text utilize the coarse-graining method, applied within the limit of a large coarse-graining factor. In this section, we explain how the coarse-graining method is applied to derive these analytical results under a plausible assumption. Initially, we introduce an assumption regarding the stabilizer tableau of a random stabilizer state, termed the *maximal scrambling ansatz*, and subsequently numerically verify this assumption. Employing the coarse-graining method in conjunction with the maximal scrambling ansatz significantly simplifies the dynamics of the tableau, thereby facilitating analytical calculations. Using these methods, we derive the results for the four-block example and the coarse-grained random circuit, as presented in the main text.

A. Random stabilizer state and maximal scrambling ansatz

When we assume a large coarse-graining factor and apply random Clifford gates, we encounter large stabilizer tableaux that consist of random stabilizers. Here, we make a plausible assumption about the stabilizer tableau of random stabilizers and numerically verify it. Consider a random stabilizer state of N qubits, which consists of K stabilizer generators g_1, g_2, \dots, g_K ($K \leq N$) that are randomly chosen assuming $N \gg 1$ and $K \gg 1$. Consequently, the

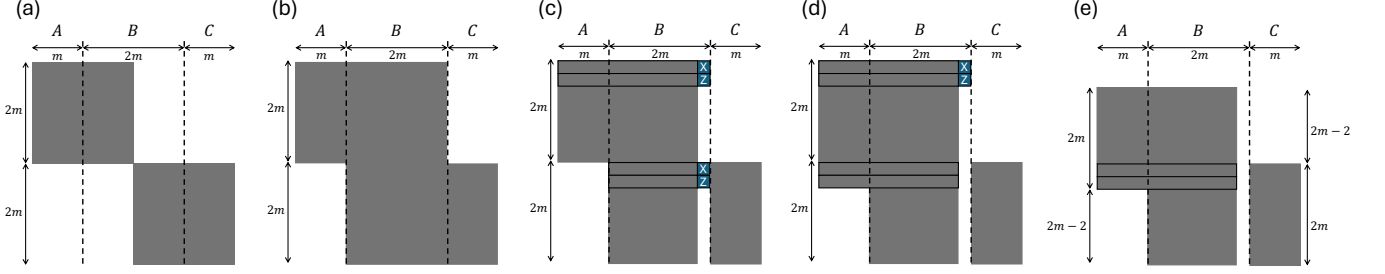


FIG. S2. (a) Stabilizer tableau after applying U_1 and U_2 . The large random Clifford gates U_1 and U_2 make the two $2m \times 2m$ block diagonals consist of random stabilizers. The random tableau entities are colored grey, and the trivial entities of $\mathbb{1}$'s are colored white. (b) Stabilizer tableau after applying U_3 . U_3 makes the rows that act nontrivially on B extend to the entire B . (c) We find two independent Pauli operators on the $3m$ -th column among the first $2m$ rows and bring them to the first two rows. Then, by doing row reductions using those rows, we make the other elements of the $3m$ -th column all $\mathbb{1}$'s for the first $2m$ -rows. We do the same task on the last $2m$ rows. (d) Stabilizer tableau after multiplying the $(2m+1)$ -th and $(2m+2)$ -th rows by the first and second rows, respectively. (e) Removing the first two rows completes the complete depolarization on $3m$ -th qubit. This results in the loss of two rows while preserving the number of rows that randomly act on A and those randomly act on C .

rows of the stabilizer tableau of this state are random Pauli strings such that (1) g_1, g_2, \dots, g_K are independent, and (2) $[g_i, g_j] = 0$ for any $i, j = 1, 2, \dots, K$. Note that this random stabilizer state is equivalent to a stabilizer state after the application of an N -qubit random Clifford gate on any stabilizer state of N qubits and K stabilizer generators.

Random Clifford gates on a large number of qubits maximally generate entanglement between any bipartition [7, 8]. This motivates us to assume that the clipped gauge of the random stabilizer state is in the *maximal scrambling ansatz*. The maximal scrambling ansatz for N qubits and K stabilizer generators denotes a stabilizer tableau in the clipped gauge comprising stabilizer generators whose lengths are all $len_{\text{ideal}} = N + K/2 + 1$. Given that every column is required to have no more than two endpoints in the clipped gauge, the stabilizer tableau of the maximal scrambling ansatz has a parallelepiped shape, as depicted in Fig. S1(a). Notably, for $i \leq N/2$, the bipartitions $A = \{1, 2, \dots, i\}$ and $B = \{i+1, i+2, \dots, N\}$ exhibit the maximal mutual information of

$$I(A : B) = \min\{2i, K\}, \quad (\text{S5})$$

by Eq. (S2). If we select A and B to be non-contiguous regions, they can be rendered contiguous by permuting the qubits, and the random stabilizer state remains invariant under such permutation. Therefore, the maximal scrambling ansatz demonstrates the maximal correlation between any bipartition.

Fig. S1(b) presents an example of a clipped gauge from a random stabilizer state with $N = 100$ qubits and $K = 70$ stabilizer generators. Here, the lengths of the stabilizer generators approximate those predicted by the maximal scrambling ansatz, with a minor deviation δ :

$$len = len_{\text{ideal}} + \delta. \quad (\text{S6})$$

Specifically, Fig. S1(c) illustrates the distribution of the lengths of the stabilizer generators. As the distributions for various values of N and K closely align, this suggests that the deviation δ is independent of N and K . Furthermore, the distribution of δ matches well with the fitting line $y = A \text{sech}^2(Bx)$, where $A = 0.3835$ and $B = 0.7762$. This indicates that a large deviation is exponentially unlikely. Therefore, the deviation δ becomes negligible compared to len_{ideal} as N increases, as demonstrated in Fig. S1(d). In the derivation of the analytical results in the main text, such fluctuations negligible to the size of the stabilizer do not affect the results. Consequently, we adopt the maximal scrambling ansatz for random stabilizer states in subsequent sections.

B. Four-block example

Equipped with the assumption of the maximal scrambling ansatz, we derive the results of the four-block example described in Fig. 2(a) in the main text. The approach of the maximal scrambling ansatz reproduces Eqs. (4) and (6) in the main text. In the four-block example, we consider a quantum circuit of four blocks of qubits, each consisting of m qubits with $m \gg 1$. We denote the first and last blocks as A and C , respectively, and the two in the middle as B . The circuit starts from the product state $|0\rangle^{\otimes 4m}$, corresponding to the $4m \times 4m$ stabilizer tableau of all Z 's on its diagonal and $\mathbb{1}$'s elsewhere. Then, we apply a $2m$ -qubit random Clifford gate U_1 on A and the left half of B , and another $2m$ -qubit random Clifford gate U_2 on the other half of B and C . The random Clifford gates U_1 and U_2 fill the

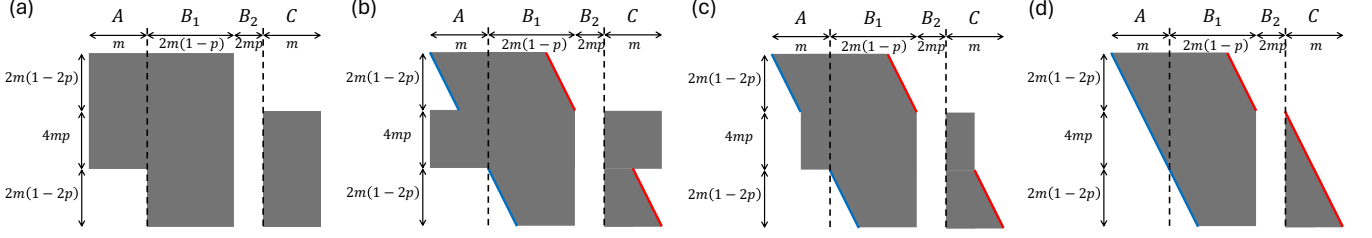


FIG. S3. Procedure of taking clipped gauge after completely depolarizing the qubits in B_2 . (a) Stabilizer tableau after depolarizing all qubits in B_2 . (b) We take maximal scrambling ansatz for the submatrices of the first $2m(1-2p)$ rows and the last $2m(1-2p)$ rows. Here, the left and right endpoints are colored blue and red, respectively. Since we take the limit of $m \gg 1$, the maximal scrambling ansatz approaches the parallelepiped shape. (c) By row reduction with the first and last $2m(1-2p)$ rows, we make the first and last $m(1-2p)$ columns of the $4mp$ rows in the middle all 1's (d) Finally, we take maximal scrambling ansatz on the submatrix of the $4mp$ rows in the middle. This results in the stabilizer tableau in the clipped gauge.

two $2m \times 2m$ block diagonals with random stabilizers, as seen in Fig. S2(a). After that, we apply another $2m$ -qubit random Clifford gate U_3 on B , which extends the stabilizer generators acting nontrivially on B across the entire B , as Fig S2(b) depicts. Finally, we completely depolarize B_2 , which consists of $2mp$ of the qubits in B , assuming $p < 1/2$. We denote the other $2m(1-p)$ qubits of B as B_1 . Due to the random Clifford gate U_3 , the choice of B_2 from B does not affect the result, and we select B_2 as the last $2mp$ qubits.

Now, we apply the complete depolarizations of the qubits in B_2 one by one, starting with the last qubit in B_2 corresponding to the $3m$ -th column. We divide the tableau into two sections—the first $2m$ rows and the others. In the first section, we find two independent Pauli operators on the $3m$ -th column—this is possible because we assume m is very large. Without loss of generality, we find two rows with X and Z , respectively, on the $3m$ -th column. By permuting rows, we bring them to the first two rows. Using these two rows for row reduction, we ensure every row of the first section, except for the first two rows, has 1 on the $3m$ -th column. We repeat this procedure on the other section. As a result, we obtain a stabilizer tableau depicted in Fig. S2(c). Then, we multiply the first and second rows of the second section by the first and second rows of the first section, respectively. As a result, the $3m$ -th column shows only 1's except for the first two rows, as seen in Fig. S2(d). Finally, eliminating the first two rows completes the complete depolarization algorithm introduced in Sec I A, resulting in the stabilizer tableau in Fig. S2(e). Consequently, the complete depolarization of a qubit in B_2 reduces the stabilizer tableau by two rows, yet preserves the number of rows randomly acting on A . The number of rows acting on C randomly remains unchanged as well. Repeating this procedure on the remaining qubits in B_2 yields the stabilizer tableau of Fig. S3(a).

For calculating $I(A : BC)$, $I(A : B)$, and $I(A : C|B)$, we take the clipped gauge. Note that the submatrix of the first $2m(1-2p)$ rows and columns of A and B_1 forms a random stabilizer state. Similarly, the submatrix of the last $2m(1-2p)$ rows and columns of B_1 and C also forms a random stabilizer state. Applying the maximal scrambling ansatz to these submatrices produces the stabilizer tableau in Fig. S3(b). Through row reduction using the first $2m(1-2p)$ rows, we convert the first $m(1-2p)$ columns of the $4mp$ middle rows to all 1's. Similarly, using the last $2m(1-2p)$ rows, we convert the last $m(1-2p)$ columns of the $4mp$ middle rows to all 1's, resulting in the stabilizer tableau in Fig. S3(c). Finally, by applying the maximal scrambling ansatz to the submatrix of the $4mp$ middle rows, we obtain the stabilizer tableau in Fig. S3(d). This series of steps, assuming maximal scrambling ansatz for the submatrices, results in the clipped gauge for the entire tableau.

Given that the stabilizer tableau in Fig. S3(d) is set in the clipped gauge, Eqs. (S2) and (S3) are applicable for calculating $I(A : B)$, $I(A : BC)$, and $I(A : C|B)$. Since A and B are adjacent, $I(A : B)$ is determined by the number of rows with left endpoints in A and right endpoints in B ,

$$I(A : B) = 2m(1-2p). \quad (\text{S7})$$

Likewise, one can see that

$$I(A : BC) = 2m, \quad (\text{S8})$$

which aligns with Eq. (6) in the main text. Subsequently, applying the chain rule of mutual information,

$$I(A : C|B) = 4mp. \quad (\text{S9})$$

Since A and C are lightcone-separated, local noise combined with random Clifford gates facilitates the rapid spreading of CMI. This phenomenon can be interpreted as selective removal of correlation due to local noise. Before depolarizing

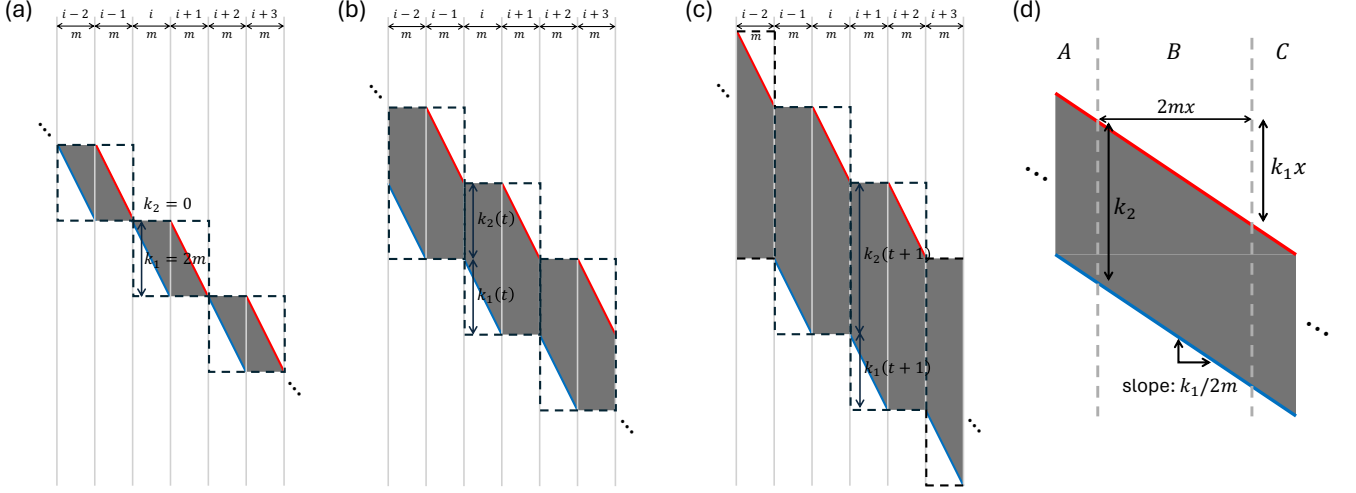


FIG. S4. (a) Stabilizer tableau after applying the first layer of the random Clifford gates on the even pairs of blocks. The box of each pair of blocks is denoted by black dashed lines. Here, $k_1 = 2m$ and $k_2 = 0$. The maximal scrambling ansatz is applied to each box. (b) Stabilizer tableau at the timestep t , with $k_1 = k_1(t)$ and $k_2 = k_2(t)$. (c) The stabilizer tableau at the timestep $t + 1$. Because of the layer of random Clifford gates at $t + 1$, the height of each box increases. (d) Stabilizer tableau after omitting the microscopic details. It consists of a diagonal stripe with the slope of $k_1/2m$ and the width of k_2 .

the qubits in B_2 , both $I(A : B)$, indicating short-range correlation, and $I(A : BC)$, indicating long-range correlation, were $4m$. Following the complete depolarization of B_2 , only short-range correlation is diminished, while long-range correlation remains unchanged. This discrepancy between short-range and long-range correlations leads to the rapid spread of CMI.

C. Coarse-grained circuit

Here, we generalize the method used to analyze the four-block example to derive the analytical results for the coarse-grained circuit, considering the limit of a large coarse-graining factor. The coarse-grained random circuit of N blocks of m qubits, depicted in Fig. 2 in the main text, begins with the initial product state $|0\rangle^{\otimes mN}$. Here, m is the coarse-graining factor that controls the local dimensionality. With N required to be even and significantly large, we apply $2m$ -qubit random Clifford gates on the even pairs of blocks $(1, 2), (3, 4), \dots, (N-1, N)$ at even time steps $t = 0, 2, \dots$, and on the odd pairs $(2, 3), (4, 5), \dots, (N-2, N-1)$ at odd time steps $t = 1, 3, \dots$. Following each random gate, we apply a heralded depolarizing channel on each qubit with an error rate p . This channel completely depolarizes the qubit with probability p , which controls the noise strength in the circuit. At every timestep, we divide the system into three regions: A , B , and C , as the first $N/2 - x$ blocks, the middle $2x$ blocks, and the last $N/2 - x$ blocks, respectively. Then, we calculate the normalized CMI, $I^{\text{norm}}(A : C|B)$, which is defined as $I(A : C|B)/m$.

Now, assuming $N \rightarrow \infty$ and $m \rightarrow \infty$, we derive Eqs. (8–10) in the main text, starting with the noiseless case where $p = 0$. The initial state $|0\rangle^{\otimes mN}$ corresponds to a stabilizer tableau with Z 's on its diagonal and $\mathbb{1}$'s elsewhere. For the stabilizer tableau at even (or odd) time steps, we assign a *box* for each even (or odd) pair of blocks. A box of the i -th and $(i+1)$ -th blocks is a submatrix comprising columns of those two blocks and rows acting nontrivially on one of the blocks. We denote the indices of the first and last rows in the box as $T_{i,i+1}$ and $B_{i,i+1}$, respectively. Additionally, we denote the number of rows with the left endpoint inside the box as k_1 and the number of the other rows as k_2 . In the large N limit, the stabilizer tableau exhibits a repeating pattern of boxes due to this translational invariance. Therefore, the indices of blocks can be omitted when denoting k_1 and k_2 . These notations allow us to show that,

$$k_1 = B_{i-2,i-1} - B_{i,i+1}, \quad (\text{S10})$$

$$k_2 = T_{i,i+1} - B_{i-2,i-1} + 1, \quad (\text{S11})$$

for $i = 1, 3, 5, \dots$ (or $i = 2, 4, 6, \dots$) at even (or odd) timesteps. For instance, in the tableau of the initial state, left and right endpoints are located on the diagonal, yielding $T_{i,i+1} = mi$ and $B_{i,i+1} = m(i+1)$ for $i = 1, 3, 5, \dots$, leading to $k_1 = 2m$ and $k_2 = 0$. The first layer of $2m$ -qubit random Clifford gates fills all boxes with random stabilizers. We apply the maximal scrambling ansatz to each box, resulting in Fig. S4(a). Notably, adopting the clipped gauge for each box results in applying the clipped gauge to the entire stabilizer tableau.

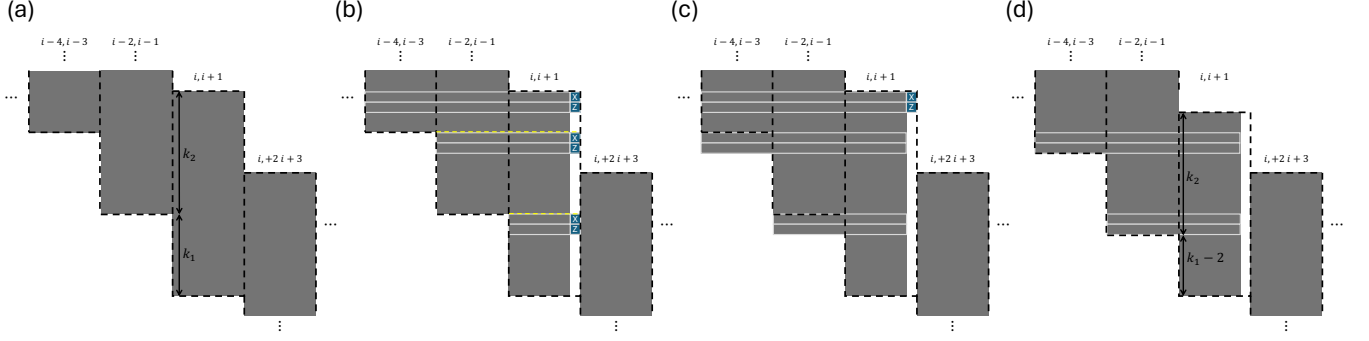


FIG. S5. Procedure of completely depolarizing the last qubit of the box of the i -th and $(i+1)$ -th blocks. (a) The stabilizer tableau where each row's support is across at most three boxes. (b) We divide the box of the i -th and $(i+1)$ -th blocks into three sections, as marked with the yellow dashed lines. On the last column of the box, we find two independent Pauli operators in each section and bring them to the first and second rows. By doing row-reduction, we make the other rows all 1s on the last column of the box. (c) The stabilizer tableau after we multiply the first two rows of the last section by the first two rows of the second section, respectively, and then multiply the first two rows of the second section by the first two rows of the first section, respectively. (d) Removing the first two rows of the box completes the complete depolarization on the last qubit of the box. This results in the reduction of k_1 by 2 while k_2 is unchanged.

To observe the stabilizer tableau's evolution, consider the tableau at timestep t with $k_1 = k_1(t)$ and $k_2 = k_2(t)$, as depicted in Fig. S4(b). Suppose the box of the i -th and $(i+1)$ -th blocks has $T_{i,i+1} = T_{i,i+1}(t)$ and $B_{i,i+1} = B_{i,i+1}(t)$. Then, at the next timestep, the box of the $(i+1)$ -th and $(i+2)$ -th blocks will have $T_{i+1,i+2}(t+1) = T_{i,i+1}(t)$ and $B_{i+1,i+2}(t+1) = B_{i+2,i+3}(t)$. Therefore, as Figs. S4(b) and (c) illustrate, $k_1(t+1) = k_1(t)$ and $k_2(t+1) = k_1(t) + k_2(t)$. The application of a layer of random Clifford gates at timestep $t+1$ fills each box with the random stabilizers. Then, subsequently taking the clipped gauge results in the tableau seen in Fig. S4(c). Consequently, the height of each box increases as k_2 grows while k_1 remains unchanged. The following equations summarize how the stabilizer tableau evolves:

$$\frac{dk_1}{dt} = 0, \quad (\text{S12})$$

$$\frac{dk_2}{dt} = k_1, \quad (\text{S13})$$

initiating with $k_1(t=0) = 2m$ and $k_2(t=0) = 0$. Therefore,

$$k_1 = 2m, \quad (\text{S14})$$

$$k_2 = 2mt. \quad (\text{S15})$$

Given $x \gg 1$, the “stair structure” of the stabilizer tableau becomes negligible. By abstracting away those microscopic details, we obtain a simplified representation of the stabilizer tableau, depicted in Fig. S4(d), with a diagonal stripe characterized by a slope of $k_1/2m$ and a vertical width of k_2 . Then, the calculation of $I(A : B)$ and $I(A : BC)$ is straightforward by leveraging the clipped gauge's properties. By Eq. (S2), $I(A : B)$ corresponds to the number of rows with left endpoints in A and right endpoints in B . With $2mx$ qubits in B ,

$$I(A : B) = \min\{k_1 x, k_2\}. \quad (\text{S16})$$

Similarly, as $I(A : BC)$ represents the number of rows with left endpoints in A and right endpoints in B or C ,

$$I(A : BC) = k_2. \quad (\text{S17})$$

Thus, we derive Eqs. (8–10) in the main text for the noiseless scenario ($p = 0$),

$$I(A : BC) = 2mt, \quad (\text{S18})$$

$$I(A : B) = \min\{2mx, I(A : BC)\}, \quad (\text{S19})$$

$$I(A : C|B) = \max\{2mt - 2mx, 0\}. \quad (\text{S20})$$

Now, we analyze the noisy case of $p > 0$. As we introduce heralded depolarizing channels, Eqs. (S12) and (S13) need to be modified accordingly. A key observation is that local depolarization decreases k_1 , but not k_2 , as long as

$t < 1/2p$. This can be demonstrated by extending the method used in the four-block example. However, unlike the four-block example, each row's support can extend across more than two boxes. Here, we demonstrate that local depolarization decreases k_1 only when each row's support spans at most three boxes, as illustrated in Fig. S5(a). Generalizing this to the cases where each row's support spans more than three boxes is straightforward.

Assuming the tableau is partitioned into boxes characterized by k_1 and k_2 before applying the clipped gauge, we first completely depolarize a single qubit in the box of the i -th and $(i+1)$ -th blocks. Without loss of generality, we choose the box's last qubit for depolarization to observe its impact on k_1 and k_2 . The box is divided into three sections: rows $T_{i,i+1}, T_{i,i+1} + 1, \dots, B_{i-4,i-3}$; rows $B_{i-4,i-3} + 1, B_{i-4,i-3} + 2, \dots, B_{i-2,i-1}$; and rows $B_{i-2,i-1} + 1, B_{i-2,i-1} + 2, \dots, B_{i,i+1}$. Similar to the four-block example, we find two independent Pauli operators on the box's last column within the first section. This is possible because of the assumption that $m \gg 1$. We locate two rows with X and Z , respectively, on the box's last column. By permuting rows, these are brought to the forefront in the first section without altering the tableau's configuration. Subsequent row reductions render all other rows in the first section as $\mathbb{1}$ on the last column. This procedure is repeated for the other sections, resulting in the stabilizer tableau shown in Fig. S5(b). After that, we multiply the first two rows of the last section by the first two rows of the second section, respectively. Again, we multiply the first two rows of the second section by the first two rows of the first section, respectively, and we get the stabilizer tableau in Fig. S5(c). Finally, deleting the first two rows of the box completes the algorithm of complete depolarization, resulting in the stabilizer tableau in Fig. S5(d). This process removes two rows from the concerned box, reducing k_1 by 2 while k_2 remains unchanged. The configurations of the other boxes stay unaltered, indicating that depolarization within a specific box does not impact the other boxes. Consequently, depolarizing a single qubit in every box diminishes k_1 by 2, maintaining k_2 constant, assuming $k_1 \geq 0$.

In the coarse-grained circuit, each timestep involves depolarizing mp qubits per block, equating to $2mp$ qubits per box. As a result, k_1 is diminished by $4mp$ at every timestep until becoming zero. This modifies the Eqs. (S12) and (S13) as follows:

$$\frac{dk_1}{dt} = -4mp, \quad (\text{S21})$$

$$\frac{dk_2}{dt} = k_1, \quad (\text{S22})$$

before k_1 becomes zero. Consequently, we derive:

$$k_1(t) = 2m(1 - 2pt), \quad (\text{S23})$$

$$k_2(t) = 2mt(1 - pt), \quad (\text{S24})$$

up until the critical timestep $t_c = 1/2p$. Employing Eqs. (S16) and (S17), we drive Eqs. (8–10) in the main text for the noisy circuit of $p > 0$,

$$I(A : BC) = 2mt(1 - pt), \quad (\text{S25})$$

$$I(A : B) = \min\{2m(1 - 2pt)x, I(A : BC)\}, \quad (\text{S26})$$

$$I(A : C|B) = \max\{2mt(1 - pt) - 2m(1 - 2pt)x, 0\}, \quad (\text{S27})$$

for $t < t_c$. At $t = t_c$, k_1 becomes zero, and $k_2 = m/2p$. This corresponds to the stabilizer tableau of $m/2p$ rows, where each row acts randomly on the entire system that consists of Nm qubits. In the next timestep, we apply complete depolarization on $\simeq Nmp$ qubits. Since we take the large N limit, all rows of the stabilizer tableau are removed, and thus, the state becomes maximally mixed. Therefore,

$$I^{\text{norm}}(A : C|B) = \begin{cases} \max\{2t(1 - pt) - 2(1 - 2pt)x, 0\}, & t \leq t_c \\ 0. & t > t_c \end{cases} \quad (\text{S28})$$

III. DETAILED NUMERICAL RESULTS

This section presents detailed numerical results, elucidating the discrepancies between analytical results and numerical simulations due to finite coarse-graining factors m and the number of blocks N . When deriving the analytical result of Eq. (S28), we assumed that both m and N are indefinitely large. However, in numerical simulations, both m and N are necessarily finite, leading to differences between the analytical and numerical results. Specifically, a finite m results in a deviation from the linear decay of CMI with respect to x , which appears in Eq. (S28), while a finite N introduces boundary effects.

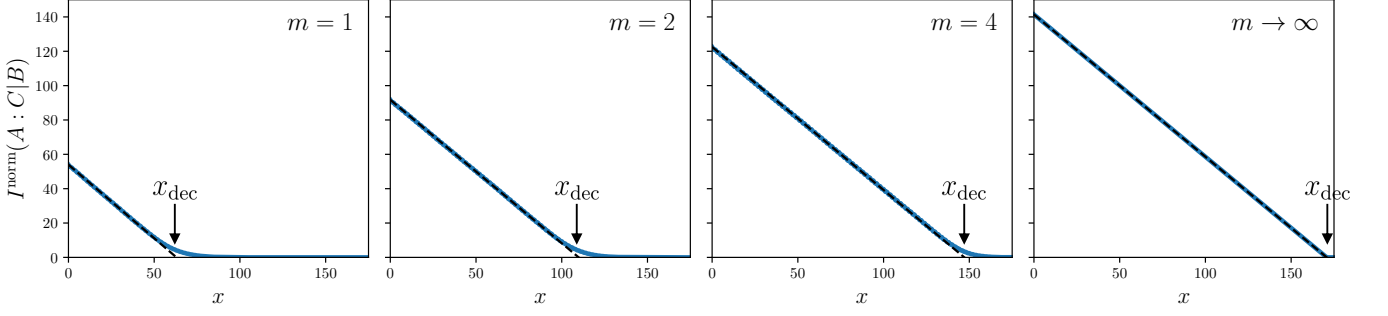


FIG. S6. Decay of $I^{\text{norm}}(A : C|B)$ in various coarse-graining factors at timestep $t = 100$. The first three panels are from the numerical results with $m = 1, 2, 4$, respectively. All numerical simulations are performed for the circuits with $N = 2^{10}$ and $p = 1.5 \times 2^{-9}$, averaged over 1000 circuit realizations. The last panel is an analytical result of (S28) with $m \rightarrow \infty$ and $p = 1.5 \times 2^{-9}$. Unlike the analytical results, $I^{\text{norm}}(A : C|B)$ has an exponential tail after the initial decay in the numerical results with the finite coarse-graining factor. Black dashed lines are the linear fittings of the initial linear decay of $I^{\text{norm}}(A : C|B)$, and x_{dec} 's are defined as the x -intercept of the fitted lines.

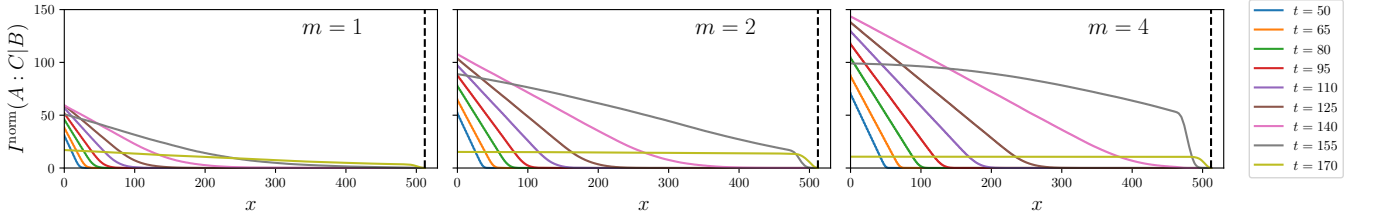


FIG. S7. Decay of $I^{\text{norm}}(A : C|B)$ at various timesteps with the coarse-graining factors 1, 2, 4, respectively. All numerical simulations are performed for the circuits with $N = 2^{10}$ and $p = 1.0 \times 2^{-9}$, averaged over 1000 circuit realizations. Black dashed lines indicate the boundary $x = N/2$. As time evolves, CMI propagates until it meets the boundary, and then the decay profile starts to be distorted.

In the theoretical model assuming $m, N \gg 1$, CMI decays linearly in terms of x until it reaches zero. In contrast, for circuits with a finite m , Fig. S6 reveals that CMI exhibits an exponential tail following the initial linear decay. This is because, although exponentially unlikely in a random circuit, there exists a constant depth quantum circuit that spreads CMI for an unbounded distance [9–12]. This exponential tail diminishes with an increase in the coarse-graining factor m and disappears in the limit as $m \rightarrow \infty$.

In the main text, for analytical results with $m \rightarrow \infty$, we define x_{dec} as the value of x at which $I^{\text{norm}}(A : C|B)$ becomes zero. However, due to the presence of the exponential tail in the decay, this definition of x_{dec} cannot be directly applied to numerical results with finite coarse-graining factors. To address this, we determine x_{dec} based on the initial linear decay. More specifically, linear fitting is performed on sections exhibiting linear decay, and the x -intercept of the fitted line is selected as x_{dec} , as illustrated in Fig. S6.

The finite value of N also creates a discrepancy between the analytical results and the numerical results, as there are

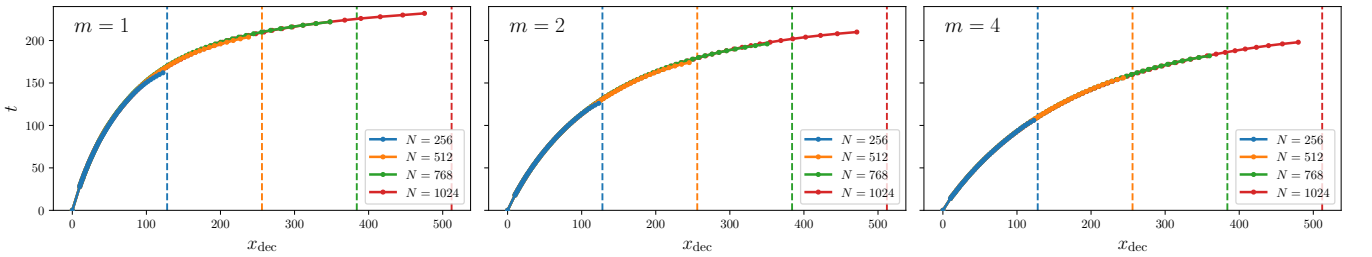


FIG. S8. Propagation of x_{dec} with the coarse-graining factors 1, 2, 4. All numerical simulations are performed for $p = 1.0 \times 2^{-9}$ with various values of N , averaged over 1000 circuit realizations. Dashed lines indicate the boundary $x = N/2$. As we omitted the distortion from the boundary, propagation of x_{dec} does not depend on N .

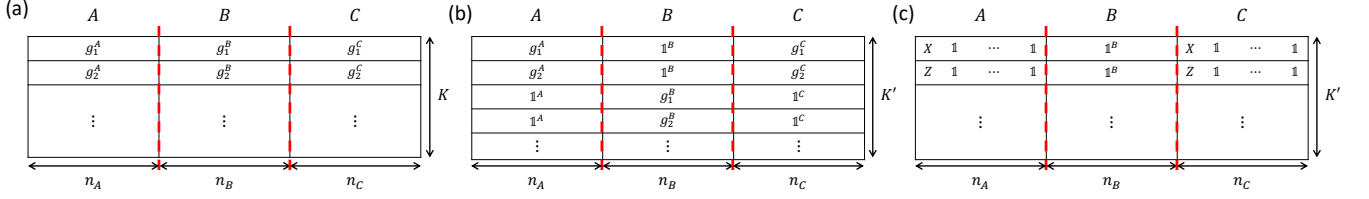


FIG. S9. (a) Stabilizer tableau of a random stabilizer state with $(n_A + n_B + n_C)$ qubits and K stabilizer generators. We divide the system into A, B, and C, which are the first n_A qubits, the second n_B qubits, and the last n_C qubits, respectively. Here, we choose g_1 and g_2 that satisfy the anticommutation conditions of Eqs. (S31) and (S32). (b) Stabilizer tableau of the state after measuring with g_1^B and g_2^B . Because of those measurements, the number of generators can increase. (c) Stabilizer tableau after the additional local operations on A and C, where A and C share a Bell pair.

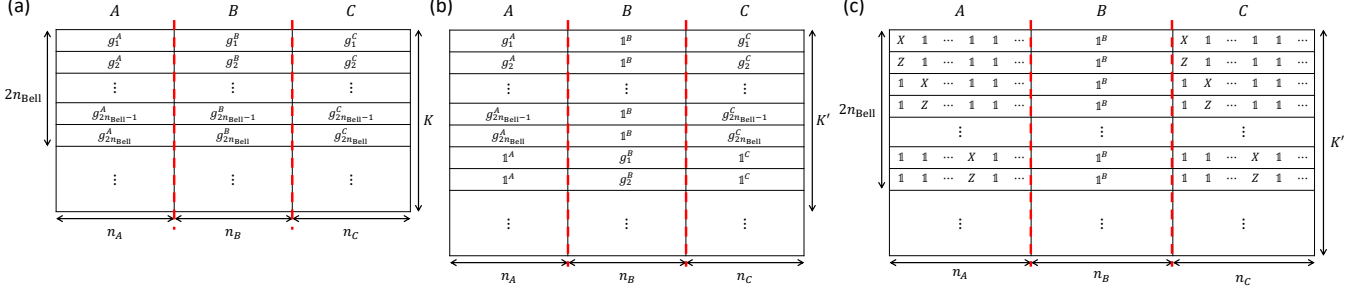


FIG. S10. (a) Stabilizer tableau of the state where there are n_{Bell} pairs of stabilizer generators $(g_1, g_2), (g_3, g_4), \dots, (g_{2n_{\text{Bell}}-1}, g_{2n_{\text{Bell}}})$ where each generator among these pairs anticommutes with the paired generator for the parts acting on A or C and commutes with the others, and all g_i^B 's commutes with each other. (b) Stabilizer tableau of the state after measuring B with $g_1^B, g_2^B, \dots, g_{2n_{\text{Bell}}}^B$. (c) Stabilizer tableau after the additional local operations on A and C, where A and C share n_{Bell} Bell pairs.

a finite number of blocks of qubits. Fig. S7 shows the effect of the boundary introduced by finite N . As CMI spreads, it eventually encounters the system's boundaries. Initially, well before reaching the boundary, CMI decays linearly, followed by an exponential tail. Once the spreading meets the boundary, the decay profile starts to be distorted. To avoid the impact of boundary-induced distortions, x_{dec} is calculated exclusively for timesteps prior to the distortion from the boundary. This approach isolates the bulk dynamics from the boundary effect. As demonstrated in Fig. S8, the propagation of x_{dec} appears independent of N , confirming that the remaining part of x_{dec} is unaffected by the boundary.

IV. GENERATING ENTANGLEMENT BETWEEN A LARGE DISTANCE

The divergence of x_{dec} at the critical timestep t_c implies CMI spreads throughout the entire system. This section demonstrates that this pervasive conditional dependence is not solely composed of classical correlations but the multipartite quantum correlation extending throughout the entire system. To see this, we show that the regions A and C, separated by an arbitrarily large region B, can achieve quantum correlation through appropriate measurements on B.

In Sec. II, we discussed the divergence of x_{dec} attributes to every stabilizer generator spanning the entire system in the clipped gauge. We consider a scenario where K stabilizer generators are left at t_c . Given these stabilizers extend across the entire system, we assume the state to be a random stabilizer state, selecting g_1, g_2, \dots, g_K as independent Pauli strings that are commuting. The system is partitioned into A, B, and C—the first n_A qubits, the second n_B qubits, and the last n_C qubits, respectively, and we write,

$$g_i = g_i^A \otimes g_i^B \otimes g_i^C, \quad (\text{S29})$$

$$(\text{S30})$$

for $i = 1, 2, \dots, K$. The stabilizer tableau is depicted in Fig. S9(a). Here, n_A , n_B , and n_C are considered indefinitely large, indicating an extensive separation between A and C.

Among those K stabilizer generators, we choose two generators, g_1 and g_2 , such that

$$g_1^A g_2^A = -g_2^A g_1^A, \quad (\text{S31})$$

$$g_1^C g_2^C = -g_2^C g_1^C. \quad (\text{S32})$$

Given that K is sufficiently large, we can choose such pairs of generators with high probability. To see this, recall that for a random stabilizer state, the stabilizer generators g_1, g_2, \dots, g_K are random Pauli strings under the constraints of $[g_i, g_j] = 0$ for $i, j = 1, 2, \dots, K$ and independence of them. However, focusing solely on the submatrix encompassing the columns for A and C , one can expect that this submatrix is insensitive to these global constraints because the significant number of columns, n_B , are neglected in Eqs. (S31) and (S32). Thus, we assume that g_i^A and g_i^B for $i = 1, 2, \dots, K$ are chosen as random Pauli strings without any constraints. Therefore, for any pairs of stabilizer generators g_i and g_j , given that non-trivial Pauli strings anti-commute with half of the elements in the Pauli group, the probability that the conditions Eqs. (S31) and (S32) are fulfilled is:

$$\frac{1}{4} (1 - 4^{-n_A}) (1 - 4^{-n_C}) \simeq \frac{1}{4}, \quad (\text{S33})$$

where factors $(1 - 4^{-n_A})$ and $(1 - 4^{-n_C})$ are for excluding the cases that we choose $g_1^A = \mathbb{1}$ or $g_1^C = \mathbb{1}$. This shows that there exists a pair of generators g_1 and g_2 satisfying the conditions Eqs. (S31) and (S32) with the probability of $\simeq 1 - (3/4)^{K(K-1)/2}$. Consequently, it is exponentially likely for us to be able to choose such g_1 and g_2 .

Here, we claim that conducting measurements on B with the observables g_1^B and g_2^B can effectively generate a Bell pair between A and C . First, the anticommutation conditions of Eqs. (S31) and (S32), alongside the constraint $[g_1, g_2] = 0$, guarantee that

$$[g_1^B, g_2^B] = 0, \quad (\text{S34})$$

so g_1^B and g_2^B are compatible observables. As mentioned in Sec. IA, the measurement outcomes only determine the overall phases of the stabilizer generators, and thus, we assume that the measurement outcomes are +1 without loss of generality. Then, the measurements make the generating set become $\{g_1, g_2, g_1^B, g_2^B, \dots\}$, possibly increasing the number of generators. We can further multiply g_1 and g_2 by g_1^B and g_2^B respectively, resulting in the stabilizer tableau in Fig. S9(b). Finally, by applying local Clifford gates on A and C , we can convert the first two rows of the tableau to $X_1 X_{n_A+n_B+1}$ and $Z_1 Z_{n_A+n_B+1}$, respectively, as seen in Fig. S9(c) [3]. Here, X_i and Z_i stand for X and Z acting on i -th qubit, respectively. Importantly, for the stabilizer state corresponding to Fig. S9(c), A and C share a Bell pair. In summary, at the critical timestep, the local observers in A and C can share a quantum entanglement by doing measurements on B and informing the measurement outcomes to A and C .

We can generalize this protocol to generate more than one Bell pair. Suppose we find $2n_{\text{Bell}}$ generators, $g_1, g_2, \dots, g_{2n_{\text{Bell}}-1}, g_{2n_{\text{Bell}}}$ such that

$$g_i^A g_{i+1}^A = -g_{i+1}^A g_i^A, \quad (\text{S35})$$

$$g_i^C g_{i+1}^C = -g_{i+1}^C g_i^C, \quad (\text{S36})$$

for $i = 1, 3, \dots, 2n_{\text{Bell}} - 1$, and

$$[g_i^A, g_j^A] = 0, \quad (\text{S37})$$

$$[g_i^C, g_j^C] = 0, \quad (\text{S38})$$

for $i, j = 1, 2, \dots, 2n_{\text{Bell}}$ such that $\{i, j\} \notin \{\{1, 2\}, \{3, 4\}, \dots, \{2n_{\text{Bell}} - 1, 2n_{\text{Bell}}\}\}$, and lastly,

$$[g_i^B, g_{i+1}^B] = 0, \quad (\text{S39})$$

$$[g_i^B, g_{i+1}^B] = 0, \quad (\text{S40})$$

for all $i, j = 1, 2, \dots, 2n_{\text{Bell}}$. In other words, there are n_{Bell} pairs of generators where each generator among those pairs anticommutes with the paired generator for the parts acting on A or C and commutes with the others, and all g_i^B 's commutes with each other. Fig. S10(a) depicts the corresponding stabilizer tableau. Then, in the same way as above, measuring B with $g_1^B, g_2^B, \dots, g_{2n_{\text{Bell}}}^B$ makes the stabilizer tableau in the form of Fig. S10(b), and we can distill n_{Bell} Bell pairs between A and C by applying local operations on A and C and thus achieving a stabilizer tableau in Fig. S10(c).

Clearly, the number of Bell pairs that are induced by the measurements on B is bounded by $K/2$, as seen in Fig S10(a). Meanwhile, at the critical timestep t_c , every stabilizer generator extends across the entire system in the clipped gauge, resulting in $I(A : C|B) = K$. Therefore, for the number of generatable Bell pairs n_{Bell} ,

$$n_{\text{Bell}} \leq I(A : C|B)/2, \quad (\text{S41})$$

at the critical timestep t_c . In other words, CMI acts as an upper bound of the number of generatable Bell pairs when $t = t_c$.

V. FURTHER DISCUSSION ON THE HERALDED DEPOLARIZING CHANNEL

To utilize the stabilizer formalism, we have adopted the heralded depolarizing channel as a decoherence model in the coarse-grained random circuit, which enables the analytical and numerical analysis. This section further discusses the heralded depolarizing channel, focusing on its difference from the depolarizing channel. First, the depolarizing channel on the qubit i with an error rate p is defined as

$$\rho \rightarrow (1 - p)\rho + p \text{Tr}_i \rho \otimes \mathbb{1}_i/2. \quad (\text{S42})$$

This noise channel describes the circumstance in which an error completely removes information in the qubit with a probability of p . Furthermore, since the output state is a mixture of the input state and the maximally mixed state, it does not reveal whether the error happened or not. On the other hand, the heralded depolarizing channel with an error rate p is defined as

$$\rho \mapsto \begin{cases} \text{Tr}_i \rho \otimes \mathbb{1}_i/2 & \text{with Prob. of } p, \\ \rho & \text{with Prob. of } 1 - p, \end{cases} \quad (\text{S43})$$

The heralded depolarizing channel also describes losing the information in the qubit with a probability of p . However, as opposed to the depolarizing channel, the output state is either the same as the input or maximally mixed state, but not a mixture of the two cases. Specifically, consider a coarse-grained random circuit with N blocks of m qubit and a depth t . Then, there are Nmt spacetime locations where we apply heralded depolarizing channels. We assign 0 and 1 to those spacetime locations as $r \in \{0, 1\}^{Nmt}$, and let ρ^r be the output state of the circuit such that we apply complete depolarization on the spacetime locations where 1 is assigned. Therefore, r indicates the configuration of the errors, and ρ^r is the output state corresponding to the configuration. Then, the circuit with the heralded depolarizing channels outputs ρ^r with the probability of $p(r) = p^{|r|}(1 - p)^{Nmt - |r|}$, where $|r|$ is the Hamming weight of r . However, if we replace the heralded depolarizing channels with depolarizing channels, the output state is $\rho^{\text{depo}} = \sum_{r \in \{0, 1\}^{Nmt}} p(r) \rho^r$.

In our study, we calculate CMI averaged over the circuit realizations. The circuit realizations depend on the choice of unitary gates and the spacetime locations of errors x , and here, we focus on taking the average over the locations of errors. First, for the circuit with the heralded depolarizing channels, we calculate the following quantity,

$$\mathbb{E}_r I(A : C|B)_{\rho^r} = \sum_{r \in \{0, 1\}^{Nmt}} p(r) I(A : C|B)_{\rho^r}, \quad (\text{S44})$$

where \mathbb{E}_r represents averaging over the locations of errors. Meanwhile, for the circuit with the depolarizing channels, we get

$$I(A : C|B)_{\rho^{\text{depo}}}. \quad (\text{S45})$$

Since CMI is not a linear function, $\mathbb{E}_r I(A : C|B)_{\rho^r}$ and $I(A : C|B)_{\rho^{\text{depo}}}$ are different in general. Moreover, there is no obvious inequality between them because CMI is neither convex nor concave.

To analyze the subtle difference between the depolarizing channel that leads to Eq. (S45) and the heralded depolarizing channel that leads to Eq. (S44), we introduce an auxiliary system R to represent the information of error locations. The auxiliary system R has an orthonormal basis $|r\rangle$ for $r \in \{0, 1\}^{Nmt}$. Let S be the qubits in the circuits, and consider a joint state of SR ,

$$\sigma_{SR} = \sum_{r \in \{0, 1\}^{Nmt}} p(r) \rho^r \otimes |r\rangle\langle r|_R. \quad (\text{S46})$$

Here, r stores the configuration of errors that outputs ρ^r . Note that if we trace out the auxiliary system R , the output state becomes that of the coarse-grained circuit with the depolarizing channels: $\rho^{\text{depo}} = \text{Tr}_R \sigma_{SR}$. Therefore,

$$I(A : C|B)_{\rho^{\text{depo}}} = I(A : C|B)_{\sigma_{SR}}. \quad (\text{S47})$$

On the other hand, for the circuit with the heralded depolarizing channels, the von Neumann entropy of a subsystem A averaged over the error configurations is

$$\mathbb{E}_r [S(A)_{\rho^r}] = \sum_{r \in \{0,1\}^{Nmt}} p(r) [-\text{Tr } \rho_A^r \log \rho_A^r] \quad (\text{S48})$$

$$= S(A|R)_{\sigma_{SR}}, \quad (\text{S49})$$

where $S(A|R)_{\sigma_{SR}} = S(AR)_{\sigma_{SR}} - S(R)_{\sigma_{SR}}$ is the conditional entropy. Since taking average $\mathbb{E}_r[\cdot]$ is linear,

$$\mathbb{E}_r [I(A : C|B)_{\rho_S^r}] = S(AB|R)_{\rho_{SR}} + S(BC|R)_{\rho_{SR}} - S(ABC|R)_{\rho_{SR}} - S(B|R)_{\rho_{SR}} \quad (\text{S50})$$

$$= I(A : C|BR)_{\rho_{SR}}. \quad (\text{S51})$$

Eqs. (S47) and (S51) clearly show that the distinction of the heralded depolarizing channel from the depolarizing channel is the extra conditioning on the auxiliary system R that contains the information of the error configuration. In other words, unlike a depolarizing channel, the heralded depolarizing channel heralds the spacetime locations of the errors, or equivalently, the spacetime locations of the errors are determined for each circuit realization. Since additional conditioning can either increase or decrease CMI [13], CMI from the circuit with the heralded depolarizing channels is neither a lower nor upper bound of that from the circuit with the depolarizing channels. Despite the difference between the depolarizing channel and the heralded depolarizing channel, they exhibit qualitative similarity when combined with random circuits [14, 15].

-
- [1] D. Gottesman, The Heisenberg Representation of Quantum Computers (1998), arXiv:quant-ph/9807006.
 - [2] S. Aaronson and D. Gottesman, Improved simulation of stabilizer circuits, *Phys. Rev. A* **70**, 052328 (2004).
 - [3] K. M. R. Audenaert and M. B. Plenio, Entanglement on mixed stabilizer states: normal forms and reduction procedures, *New J. Phys.* **7**, 170 (2005).
 - [4] A. Nahum, J. Ruhman, S. Vijay, and J. Haah, Quantum Entanglement Growth under Random Unitary Dynamics, *Phys. Rev. X* **7**, 031016 (2017).
 - [5] Y. Li, X. Chen, and M. P. A. Fisher, Measurement-driven entanglement transition in hybrid quantum circuits, *Phys. Rev. B* **100**, 134306 (2019).
 - [6] S. Sang, Z. Li, T. H. Hsieh, and B. Yoshida, Ultrafast Entanglement Dynamics in Monitored Quantum Circuits, *PRX Quantum* **4**, 040332 (2023).
 - [7] J. Preskill, Lecture notes for physics 219: Quantum Computation (2018).
 - [8] H. Apel, T. Kohler, and T. Cubitt, Holographic duality between local Hamiltonians from random tensor networks, *J. High Energ. Phys.* **2022** (3), 52.
 - [9] L. Zou and J. Haah, Spurious long-range entanglement and replica correlation length, *Phys. Rev. B* **94**, 075151 (2016).
 - [10] D. J. Williamson, A. Dua, and M. Cheng, Spurious Topological Entanglement Entropy from Subsystem Symmetries, *Phys. Rev. Lett.* **122**, 140506 (2019).
 - [11] K. Kato and F. G. S. L. Brandão, Toy model of boundary states with spurious topological entanglement entropy, *Phys. Rev. Research* **2**, 032005 (2020).
 - [12] I. H. Kim, M. Levin, T.-C. Lin, D. Ranard, and B. Shi, Universal Lower Bound on Topological Entanglement Entropy, *Phys. Rev. Lett.* **131**, 166601 (2023).
 - [13] T. M. Cover and J. A. Thomas, *Elements of information theory*, 2nd ed. (Wiley-Interscience, Hoboken, N.J, 2006).
 - [14] K. Noh, L. Jiang, and B. Fefferman, Efficient classical simulation of noisy random quantum circuits in one dimension, *Quantum* **4**, 318 (2020).
 - [15] Z. Li, S. Sang, and T. H. Hsieh, Entanglement dynamics of noisy random circuits, *Phys. Rev. B* **107**, 014307 (2023).